

Electronic Supplementary Information for

Top-Down Manufacturing Gasification Residue Carbon as Efficient CO₂ Reduction Catalyst

Jun Liu,^{1,2} Guiru Zhang,² Ke Ye,² Ke Xu,³ Yeliang Sheng,⁴ Can Yu,⁵ Hai Zhang,² Qiaoxia Li,^{1,*}
Zheng Liang,^{4,*} Kun Jiang^{2,*}

¹ Shanghai Key Laboratory of Materials Protection and Advanced Materials in Electric Power, College of Environmental and Chemical Engineering, Shanghai University of Electric Power, Shanghai 200090, China.

² Interdisciplinary Research Center, School of Mechanical Engineering, Shanghai Jiao Tong University, Shanghai 200240, China.

³ Research Institute of Petroleum Processing, Sinopec, Beijing 100083, China.

⁴ Laboratory of Energy Chemical Engineering, Frontiers Science Center for Transformative Molecules, School of Chemistry and Chemical Engineering, Shanghai Jiao Tong University, Shanghai, 200240, China.

⁵ Institute of High Energy Physics, Chinese Academy of Science, Beijing 100049, China.

* To whom correspondence should be addressed: K. Jiang (Email: kunjiang@sjtu.edu.cn), Z. Liang (Email: liangzheng06@sjtu.edu.cn) or Q. Li (Email: liqiaoxia@shiep.edu.cn)

Methods

Material synthesis. The gasification residual carbon was collected in an entrained flow gasifier using de-oiled asphalt as feedstock at Fujian Union Petrification, vacuum dried overnight for further useage. Before the pyrolysis, the as-received carbon was ground with urea (AR, Sinopharm) at a mass ratio of 1:0, 1:5 or 1:10. The mixture was then heated up to 550, 650 or 850 °C within 60 min in a tube furnace under an Ar flow of 100 sccm (99.999%, Shanghai Coogee), kept at the same temperature for another 60 min before cooling down to room temperature, and annotated as annealed residual carbon. The leached sample was prepared by dispersing the annealed carbon into 0.25 M H₂SO₄, mechanically stirred for 24 h at 80 °C to remove metal particles and unstable species.

Material characterizations. Transmission electron microscopy (TEM) was performed on a Tecnai G² F20 S-Twin transmission electron microscope at 200 kV to characterize the morphology. Aberration-corrected high angle annular dark field scanning TEM (HAADF-STEM) images were recorded a ThermoFisher Themis Z microscope equipped with two aberration correctors under 300 kV, using a convergence semi angle of 25 mrad, an inner- and outer collection angle of 47 and 200 mrad, respectively. Energy dispersive X-ray spectroscopy (EDS) was carried out using 4 in-column Super-X detectors.

X-ray photoelectron spectroscopy (XPS) was obtained with a Thermo Fisher Scientific Nexsa spectrometer, using a monochromatic Al K α radiation and a low energy flood gun as neutralizer. The binding energies were calibrated by referencing to C 1s peak at 284.8eV. Avantage XPS program was employed for surface component analysis. X-ray absorption fine structure (XAFS) spectroscopy was carried out using the *RapidXAFS* 2M (Anhui Absorption Spectroscopy Analysis Instrument Co., Ltd.) by transmission mode at 20 kV and 40 mA, and a Si (551) spherically bent crystal analyzer with a radius of curvature of 500 mm. Analyses of both the near edge (in energy scale) and extended range (in *R* space) XAFS spectra were performed using the IFEFFIT-based Athena program.

Inductively coupled plasma optical emission spectrometry (ICP-OES) was measured on a Thermo Scientific iCAP-Q spectrometer to quantify the metal ratio. XRD spectra were recorded on a Burker-AXS D8 Advance spectrometer using a Cu K α radiation (40 kV, 40 mA) at a scan rate of 0.02° per step and a holding time of 1 s per step. The N₂ adsorption and desorption was measured at 77 K liquid nitrogen atmosphere using a 4-station automatic specific surface area analyzer model APSP-2460 from Micromeritics, USA, and the total BET specific surface area of the material was calculated by the BET method.^{1,2} Prior to each measurement, the residual carbon powders were pre-treated under vacuum at 350 °C for 12 h using the standard degassing station

of Micromeritics. The Raman spectra were collected on a Horiba LabRAM HR Evolution confocal Raman microscopy, using a 633-nm Ventus VIS laser excitation and a 50× objective, with a dispersion grating of 600 g mm⁻¹.

Electrochemical measurements. The electrochemical measurements were run at 25 °C in a customized gastight H-type glass cell separated by a Nafion 117 membrane (Fuel Cell Store). A BioLogic VMP3 workstation was employed to record the electrochemical response. A certain amount of Cs₂CO₃ (99.95%, Sigma-Aldrich) was dissolved in Millipore water to prepare a 0.05 M electrolyte, which was further purified by electrolysis between two graphite rods at 0.1 mA for 24 h to remove any trace amounts of metal ions. In a typical 3-electrode test system, a platinum mesh electrode (99.99%, Gauss Union) and a saturated calomel electrode (SCE, CH Instruments) were used as the counter and reference electrodes, respectively. A fresh (electrochemically) polished glassy carbon (Gauss Union, 1×2 cm²) was used as the working electrode substrate.

Typically, 5 mg of the residual carbon with different treatment was mixed with 1 mL of ethanol and 100 μL of a Nafion 117 solution (5%, Sigma-Aldrich), and sonicated for 20 min to get a homogeneous catalyst ink. 80 μL of the ink was pipetted onto a 2 cm² glassy carbon surface (0.2 mg cm⁻² mass loading), which was vacuum dried prior to use. All potentials measured against the SCE were converted to the reversible hydrogen electrode (RHE) scale in this work using E (vs. RHE) = E (vs. SCE) + 0.244 V + 0.0591×pH, where the pH value of 0.1 M CO₂-saturated CsHCO₃ was determined as 6.8. The solution resistance (R_s) was determined by potentiostatic electrochemical impedance spectroscopy (PEIS) at frequencies ranging from 0.1 Hz to 200 kHz, and manually compensated at 85% level for the CO₂RR measurements in H-cell.

For an anion membrane electrode assembly measurement, ca. 0.5 mg cm⁻² leached residual carbon and 1.8 mg cm⁻² IrO₂ (P40V020, Premetek Co.) were air-brushed onto two 2.5×2.5 cm² Toray TGP-H-060 carbon paper as CO₂RR cathode and OER anode, respectively. A quaternary ammonia poly(N-methyl-piperidine-*co-p*-terphenyl) (QAPPT, EVE Energy) anion exchange membrane was sandwiched in between the two gas diffusion layer electrodes to separate the chambers. The QAPPT membrane was pre-activated in 1 M KOH at 60 °C for 24 h before useage. On the cathode side, 50 sccm humidified CO₂ was fed through a titanium gas flow channel, while the anode was circulated with 0.1 M CsHCO₃ electrolyte at a flow rate of 2 mL min⁻¹.³ The cell voltage was recorded without iR -correction.

CO₂RR products quantification. The effluent from the electrochemical cell was analyzed by a Shimadzu 2014 gas chromatography (GC) equipped with a thermal conductivity detector (TCD) for H₂ concentration quantification and a flame ionization detector (FID) coupled with a

methanizer for quantifying CO concentration. UHP Ar was used as the carrier gas and constituents of the gaseous sample were separated using two Porapak N80/100 columns packed with Molecular Sieve-13X. The signal response of the TCD and FID were calibrated by analyzing a series of standard gas mixtures (Wetry, H₂ concentrations of 50.6, 505, 7557, 101000 ppm and CO concentrations of 20.3, 203, 7510, 50100 ppm). Faradaic efficiency (FE) of certain reduction product was calculated as:

$$FE = \frac{x_i \nu n F}{V \times j} \times 100\%$$

where x_i is the volume fraction of specie i as determined by on-line GC, ν is the flow rate set at 20 sccm and being controlled by an Alicat mass flow controller, n is the electron transfer number, F is the Faradaic constant, V is the molar volume of ideal gas under CO₂RR operation condition, j is the total current density.

Computational details. All the calculations are performed in the framework of the density functional theory (DFT) with the projector augmented plane-wave method, as implemented in the Vienna ab initio simulation package.⁴ The generalized gradient approximation proposed by Perdew, Burke, and Ernzerhof is selected for the exchange-correlation potential.⁵ The Grimme D3 correction using a coordination number dependent dispersion correction.⁶ The cut-off energy for plane wave is set to 450 eV. The energy criterion is set to 10⁻⁵ eV in iterative solution of the Kohn-Sham equation. A vacuum layer of 15 Å is added perpendicular to the sheet to avoid artificial interaction between periodic images. The Brillouin zone integration is performed using a 2×2×1 k-mesh.⁷ All the structures are relaxed until the residual forces on the atoms have declined to less than 0.03 eV/Å.

The formation energies (E_f) of the Ni atom doped in the vacancies of graphene could be calculated by the following:

$$\Delta E_f = \Delta E_{FS} - \Delta E_{IS} - \Delta E_{H_2}$$

where ΔE_f is the formation energies on the surface from DFT calculations. The ΔE_{IS} and ΔE_{FS} are the energy of the initial state (IS) and final state (FS) of the metal atoms in the cluster intercalated into the graphite to form a single-atom coordination. The ΔE_{H_2} is the energy of a H₂ molecule that was used to neutralize the unsaturated sites on graphite.

Supplementary Figures

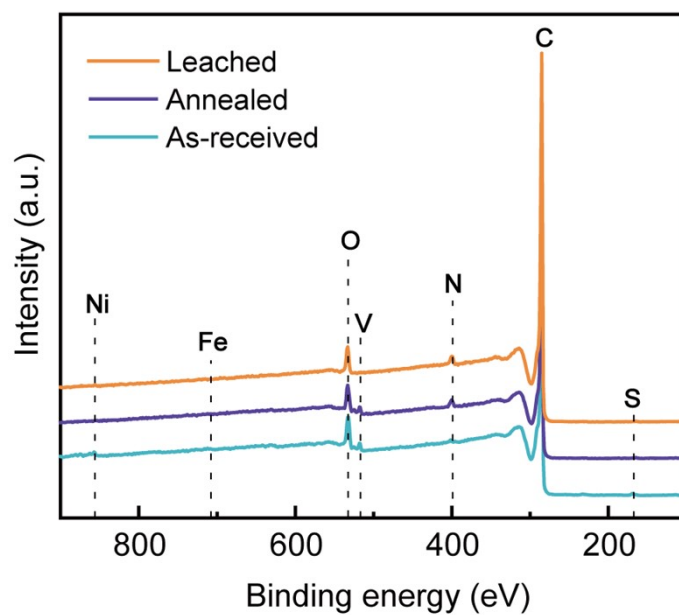


Fig. S1 XPS survey spectra for as-received, annealed and leached residual carbon catalysts.

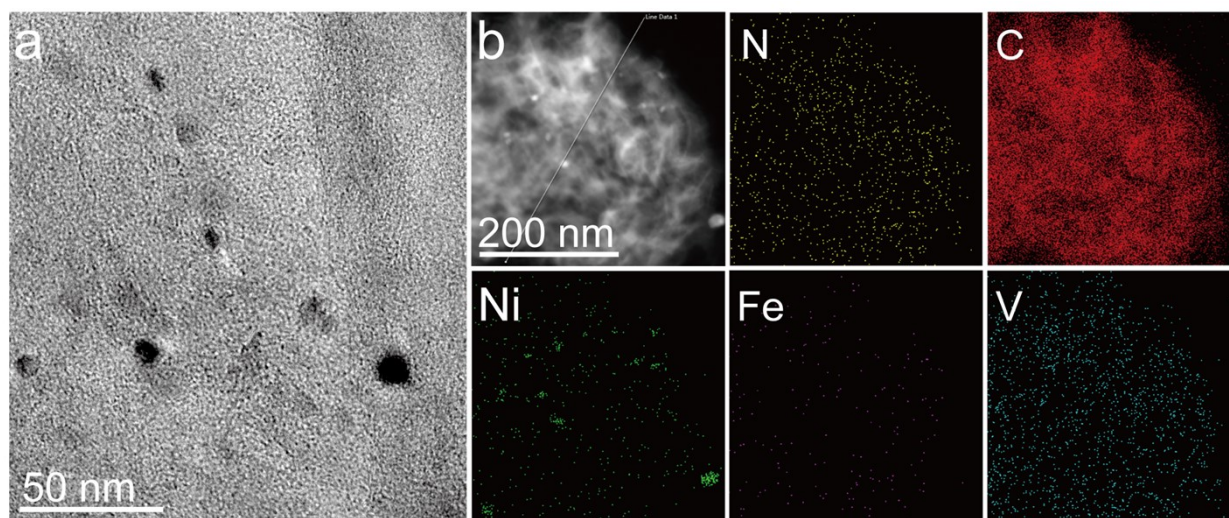


Fig. S2 (a) TEM images of annealed residual carbon, together with (b) relevant EDS mapping. Individual Ni nanoparticles were identified, with a homogeneous distribution of V and trace amount of Fe components.

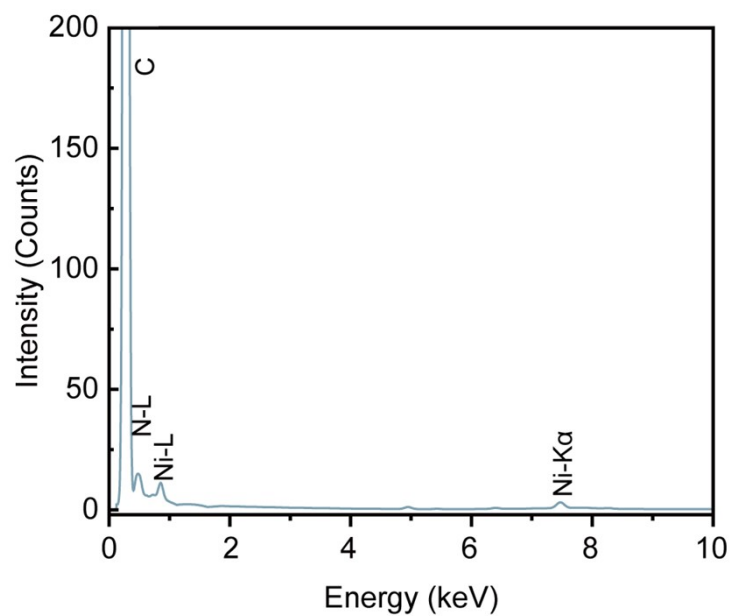


Fig. S3 The EDS spectra of leached catalyst, relevant mapping results were plotted in Fig. 1 of main text.

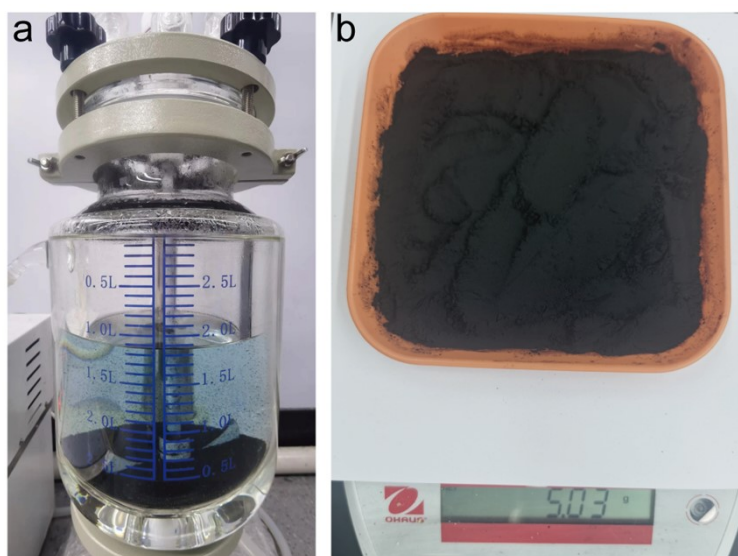


Fig. S4 (a) Photograph of acidic leaching treatment, (b) the obtained ~5 g single atom catalysts in one batch synthesis.

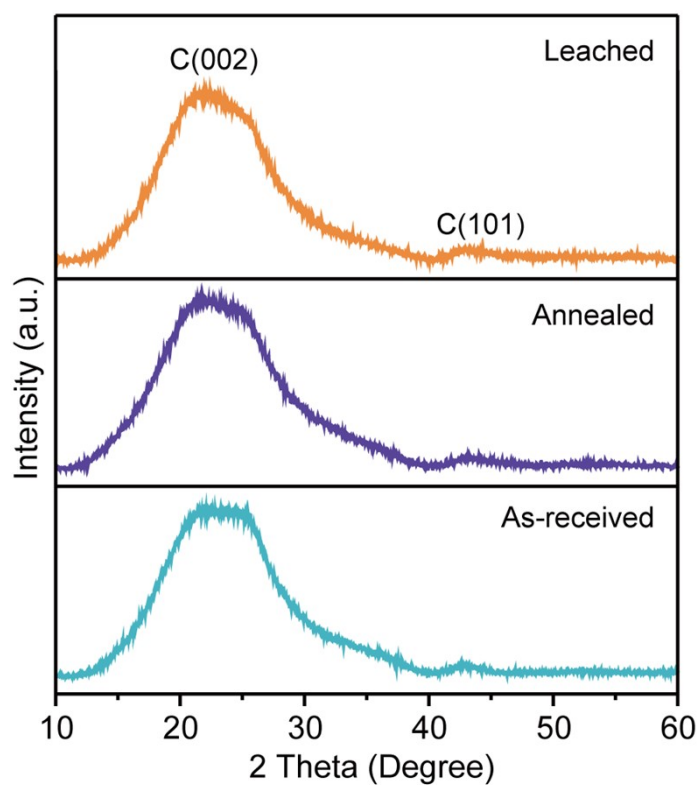


Fig. S5 XRD patterns of as-received, annealed and leached residual carbon powders.

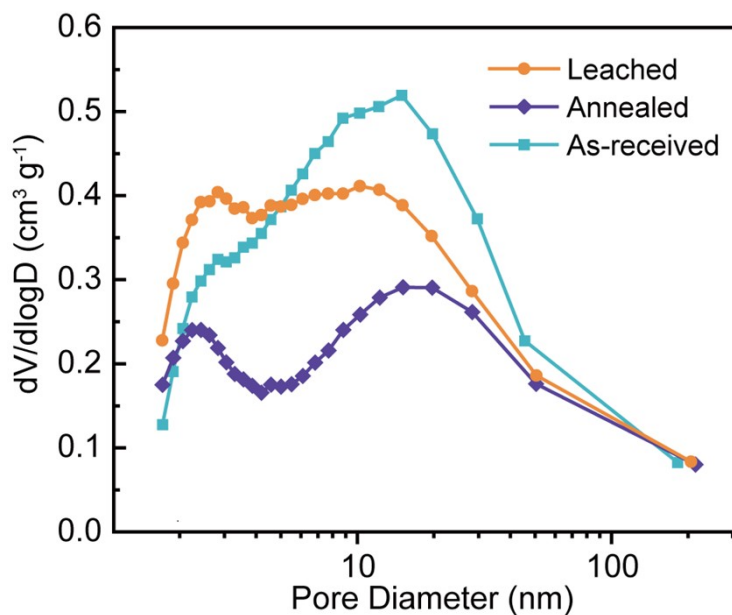


Fig. S6 Comparison of the pore size distribution of residual carbon catalysts. After pyrolysis, the metallic constituents undergo thermal growth and agglomeration to form metal oxide nanoparticles, which consume part of the pores. Thereafter, the pores could be released after the acidic leaching that completely removes the metal oxide nanoparticles.

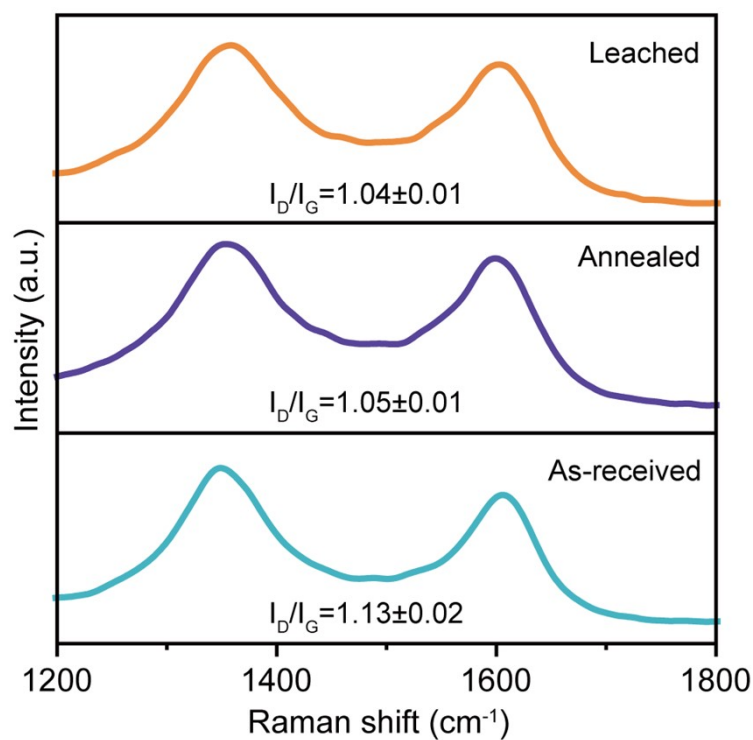


Fig. S7 Representative Raman spectra of as-received, annealed and leached residual carbon powders. The statistical errors represent two independent measurements.

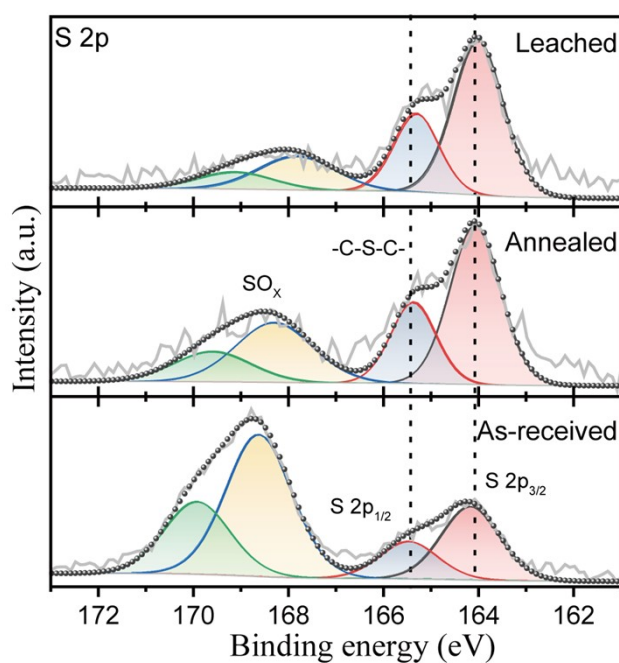


Fig. S8 The core-level XPS spectra on S 2p region for as-received, annealed and leached residual carbon. The two sets of S characteristic peaks can be ascribed to $-\text{SO}_x$ and C-S-C species, respectively.⁸

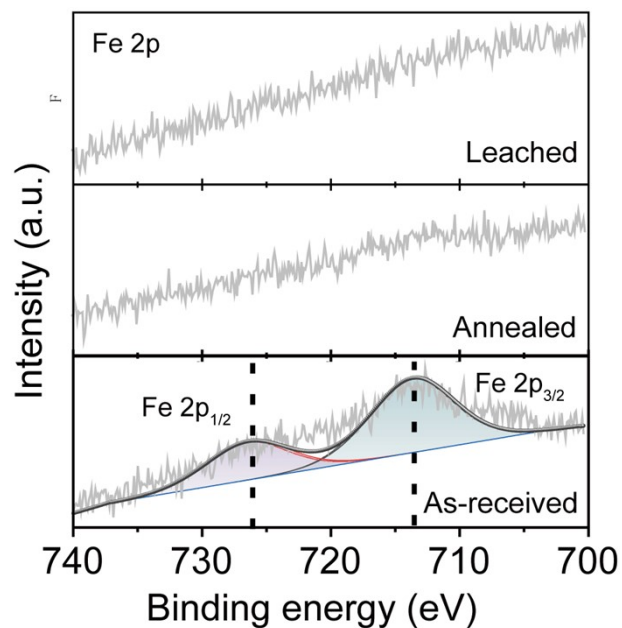


Fig. S9 The core-level XPS spectra on Fe 2p region for as-received, annealed and leached residual carbon. The Fe 2p_{3/2} binding energy locates at ~713.6 eV for as-received carbon, probably ascribing to the Fe₂O₃ component.⁹

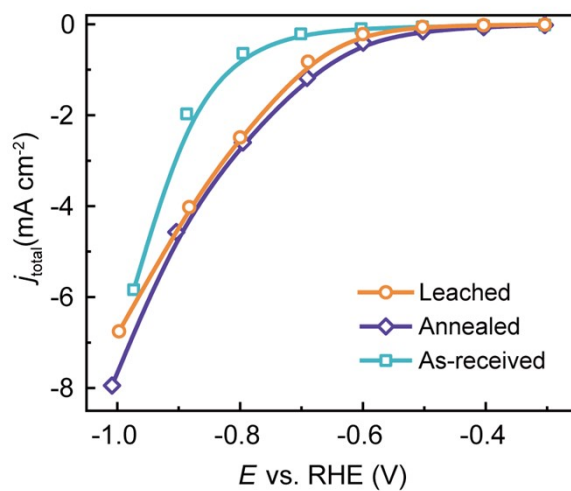


Fig. S10 The steady-state current densities recorded on catalysts-cast glassy carbon electrodes in CO₂-saturated 0.1 M CsHCO₃.

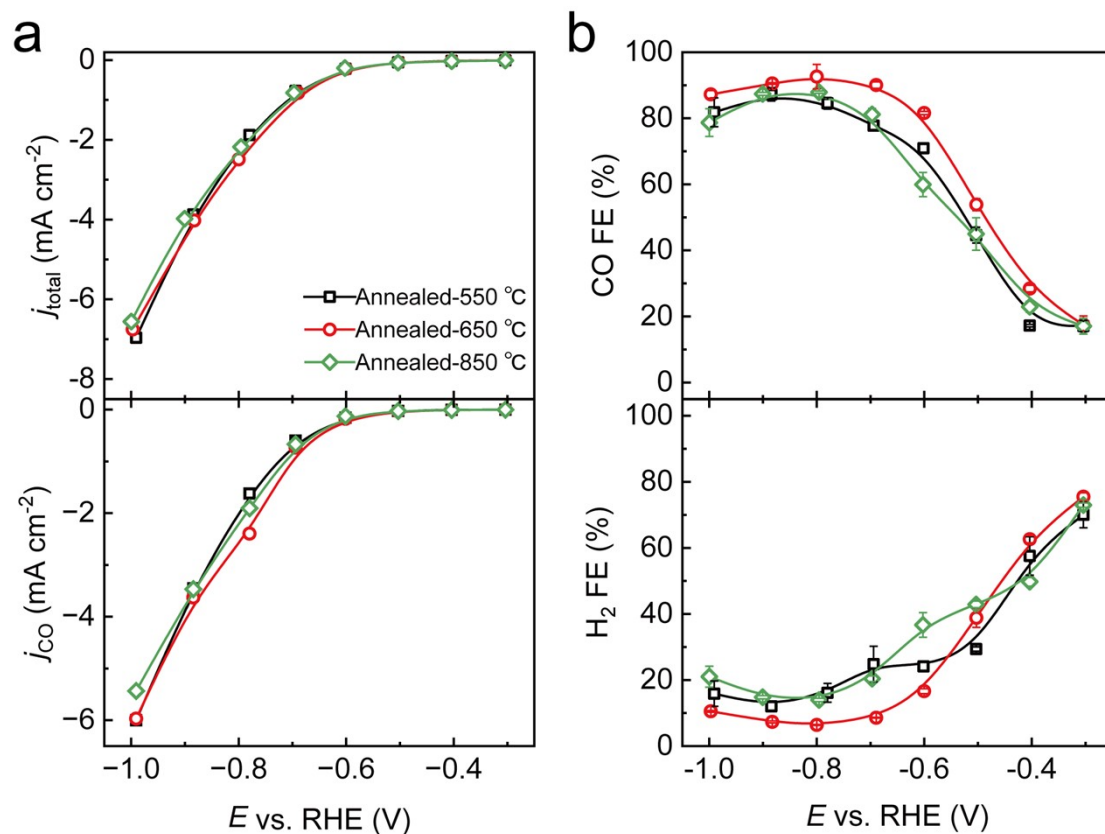


Fig. S11 The effect of annealing temperature on the CO₂RR performance. (a) Steady-state Faradaic current densities and CO partial current densities, (b) the corresponding FEs for H₂ and CO. Note: a pretreatment of diluted H₂SO₄ washing was carried out for each annealed carbon annealed at different temperatures prior to the electrochemical CO₂RR measurements.. The error bars represent two independent measurements.

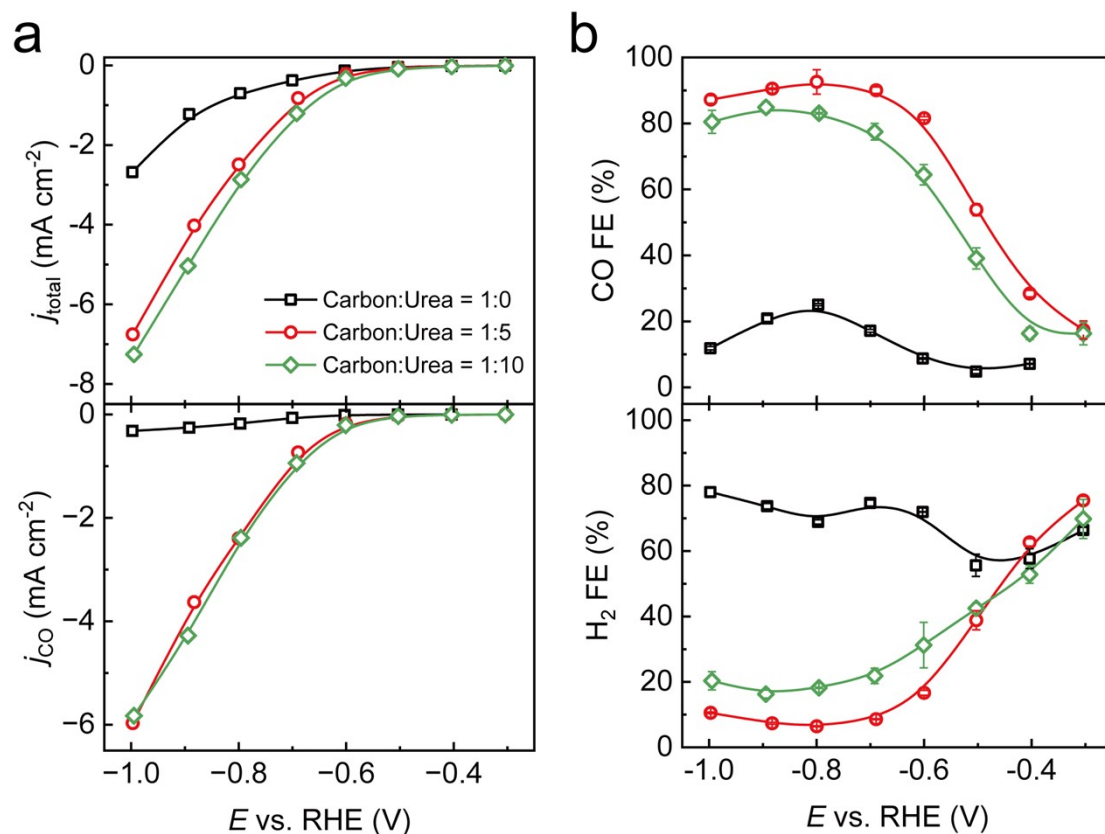


Fig. S12 The effect of urea amount added during co-pyrolysis on the CO₂RR performance. (a) Steady-state Faradaic current densities and CO partial current densities, (b) the corresponding FEs for H₂ and CO. Note: a pretreatment of diluted H₂SO₄ washing was carried out for each annealed carbon annealed at different temperatures prior to the electrochemical CO₂RR measurements. The error bars represent two independent measurements.

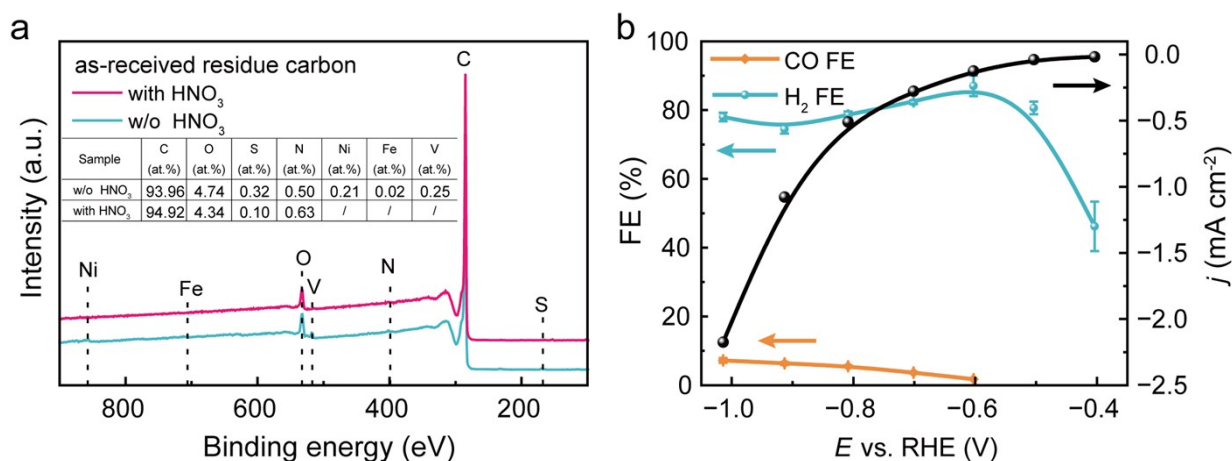


Fig. S13 (a) Comparison of XPS survey spectra for as-received residual carbon with or without 5 M HNO₃ hot-bath treatment at 90 °C for 5 h under stirring. (b) The steady-state current density at each applied potential and the corresponding FEs for CO and H₂ recorded on HNO₃-treated as-received carbon catalyst.

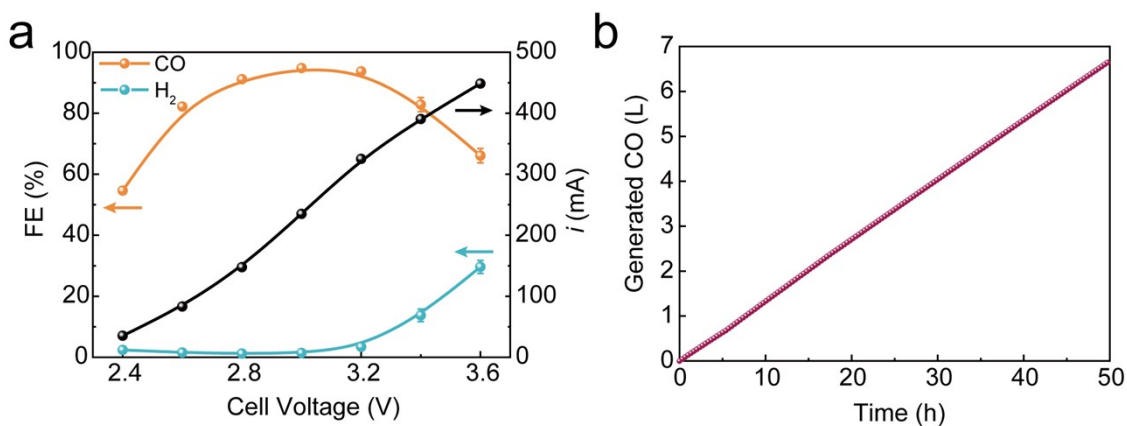


Fig. S14 CO₂RR performance as delivered by leached residual carbon in a home-built 2.5×2.5 cm² AEM electrolyzer. (a) The steady-state current at each applied voltage and the corresponding FEs for CO and H₂, and (b) accumulated CO volume during the 50-h continuous electrolysis at a constant current of 300 mA. The error bars represent two independent measurements.

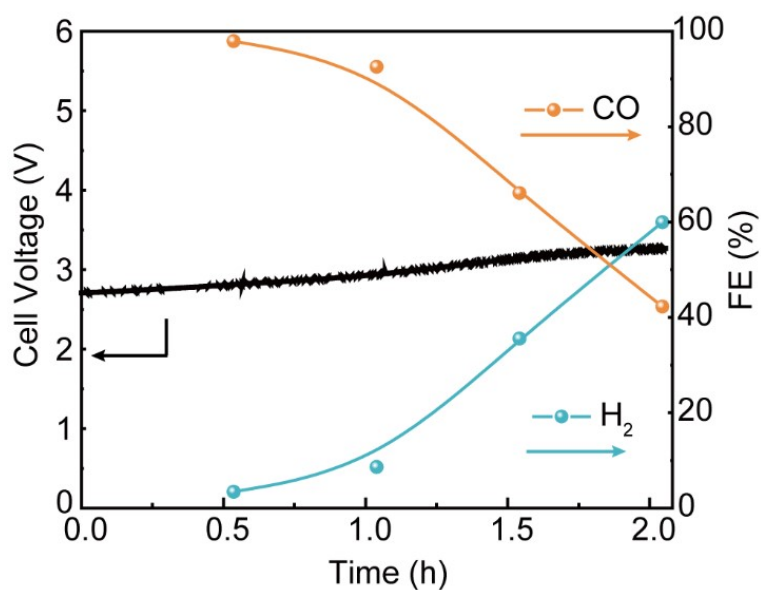


Fig. S15 Long-term electrolysis of annealed residue carbon (without acidic leaching treatment) cast cathode at a constant current of 300 mA within an AEM model electrolyzer, in which a rapid decay of CO Faradaic efficiency and cell voltage were noted.

Supplementary Tables

Table S1. ICP-OES results on different batch of residue carbon from the same gasifier at Fujian Union Petrification.

Entry	Date of Residue Carbon Collected	Fe (wt.%)	Ni (wt.%)	V (wt.%)	Ca (wt.%)
1#	2021.08.25	0.650	1.190	3.080	/
2#*	2022.02.24	0.092	0.635	2.252	/
3#	2022.10.12	0.201	0.947	2.927	0.015

* Gasification residue carbon in the **2# Batch** (~10 kg) was used throughout the present work.

Table S2. The determined weight content and atomic content for residual carbons as derived from ICP-OES.

Sample	Fe		Ni		V	
	(wt.%)	(at.%)	(wt.%)	(at.%)	(wt.%)	(at.%)
As-received	0.092	0.020	0.635	0.130	2.252	0.531
Annealed	0.090	0.019	0.463	0.095	2.845	0.671
Leached	0.017	0.004	0.186	0.038	0.060	0.014

Table S3. The determined atomic content as derived from XPS survey spectra.

Sample	C (at.%)	O (at.%)	S (at.%)	N (at.%)	Ni (at.%)	Fe (at.%)	V (at.%)
As-received	93.96	4.74	0.32	0.50	0.21	0.02	0.25
Annealed	93.69	4.00	0.13	1.74	0.14	/	0.30
Leached	94.02	3.67	0.09	1.89	0.12	/	/

Table S4. Textural properties of as-received, annealed and leached residual carbon catalysts. *

Sample	S_{BET} (m ² /g)	V_{micro} (×10 ⁻¹ cm ³ /g)	V_{T} (×10 ⁻¹ cm ³ /g)	D_{P} (nm)
As-received	349.8	0.10	7.36	8.4
Annealed	275.7	0.04	4.92	8.6
Leached	435.1	0.15	6.77	7.1

* S_{BET} is the specific surface area determined by the BET method. V_{micro} is the micropore volume obtained using the t-plot method. V_{T} and D_{P} are respectively, the total pore volume and average pore diameter calculated by means of the BJH method from the adsorption branch of N₂ isotherm.

Table S5. Detailed parameters for the core-level XPS spectra fitting.

Sample	XPS Peak		Position (eV)	FWHM (eV)	Area (eV)	
As-received	N 1s		401.6	2.8	3321.6	
	S	C-S-C	2p _{3/2}	163.9	1.5	607.9
			2p _{1/2}	165.5	1.5	310.5
		-SO _x	2p _{3/2}	168.6	1.7	1323.4
			2p _{1/2}	169.9	1.7	676
	Ni	2p _{3/2}	856.8	2.5	5754	
		2p _{1/2}	874.1	3.2	2900	
	V	2p _{3/2}	517.4	1.6	6698.6	
		2p _{1/2}	524.8	2.8	3617.2	
	Fe	2p _{3/2}	713.6	3.5	942.2	
		2p _{1/2}	726.4	3.5	986.4	
	Annealed	S	C-S-C	2p _{3/2}	164.1	1.3
2p _{1/2}				165.4	1.2	183.7
-SO _x			2p _{3/2}	168.3	2.0	231.1
			2p _{1/2}	169.6	2.0	118.1
N 1s		pyridine-N	398.8	1.7	4353.9	
		N-M	400.1	1.7	3440.1	
		pyrrolic-N	401.6	1.8	2298.1	
		quaternary-N	403.5	1.8	908.7	
		oxidized-N	405.8	2.0	609.4	
Ni		2p _{3/2}	855.8	3.0	1308.6	
		2p _{1/2}	873.1	3.0	678	
V		2p _{3/2}	517.2	1.9	7169.6	
		2p _{1/2}	524.6	3.2	3656.5	
Leached		S	C-S-C	2p _{3/2}	164	1.3
	2p _{1/2}			165.3	1.2	188.3
	-SO _x		2p _{3/2}	167.8	2.0	139.5
			2p _{1/2}	169.1	2.0	71.3
	N 1s	pyridine-N	398.6	1.7	5329.3	
		N-M	400.1	1.7	4508.4	
		pyrrolic-N	401.4	1.8	2515.7	
		quaternary-N	403.3	1.8	1086.8	
		oxidized-N	405.4	2.0	543.9	
	Ni	2p _{3/2}	856.3	3.5	1963.1	
		2p _{1/2}	873.6	3.5	1017.2	

Supplementary References

1. S. Brunauer, P.H. Emmett, E. Teller, *J. Am. Chem. Soc.*, 1938, **60**, 309-319.
2. E. P. Barrett, L. G. Joyner, P. P. Halenda, *J. Am. Chem. Soc.*, 1951, **73**, 373-380.
3. K. Ye, G. Zhang, X.-Y. Ma, C. Deng, X. Huang, C. Yuan, G. Meng, W.-B. Cai and K. Jiang, *Energy Environ. Sci.*, 2022, **15**, 749-759.
4. G. Kresse and D. Joubert, *Phys. Rev. B*, 1999, **59**, 1758-1775.
5. J. P. Perdew, K. Burke and M. Ernzerhof, *Phys. Rev. Lett.*, 1996, **77**, 3865-3868.
6. S. Grimme, J. Antony, S. Ehrlich and H. Krieg, *J. Chem. Phys.*, 2010, **132**, 154104.
7. D. Bende, F. R. Wagner, O. Sichevych and Y. Grin, *Angew. Chem. Int. Edit.*, 2017, **129**, 1333-1338.
8. M. A. Hoque, F. M. Hassan, A. M. Jauhar, G. Jiang, M. Pritzker, J.-Y. Choi, S. Knights, S. Ye and Z. Chen, *ACS Sustain. Chem. Eng.*, 2018, **6**, 93-98.
9. A. P. Grosvenor, B. A. Kobe, M. C. Biesinger and N. S. McIntyre, *Surf. Interface Anal.*, 2004, **36**, 1564-1574.